

Blade vibration study by spectral analysis of tip-timing signals with OMP algorithm

Antoine Bouchain, José Picheral, Elisabeth Lahalle, Gilles Chardon, Agathe Vercoutter, Arnaud Talon

▶ **To cite this version:**

Antoine Bouchain, José Picheral, Elisabeth Lahalle, Gilles Chardon, Agathe Vercoutter, et al.. Blade vibration study by spectral analysis of tip-timing signals with OMP algorithm. Mechanical Systems and Signal Processing, 2019, 130, pp.108-121. 10.1016/j.ymssp.2019.04.063 . hal-02125263

HAL Id: hal-02125263

https://centralesupelec.hal.science/hal-02125263

Submitted on 10 May 2019

HAL is a multi-disciplinary open access archive for the deposit and dissemination of scientific research documents, whether they are published or not. The documents may come from teaching and research institutions in France or abroad, or from public or private research centers.

L'archive ouverte pluridisciplinaire **HAL**, est destinée au dépôt et à la diffusion de documents scientifiques de niveau recherche, publiés ou non, émanant des établissements d'enseignement et de recherche français ou étrangers, des laboratoires publics ou privés.

Blade vibration study by spectral analysis of tip-timing signals with OMP algorithm

Antoine Bouchain[a,b], José Picheral[a], Elisabeth Lahalle[a], Gilles Chardon[a], Agathe Vercoutter[b], Arnaud Talon[b]

[a] *Laboratoire des Signaux et Systèmes*
CentraleSupélec - CNRS - Université Paris Sud - Université Paris Saclay,
3 Rue Joliot-Curie, 91192 Gif sur Yvette, France
[b] *Safran Helicopter Engines,*
Avenue Joseph Szydlowski, 64510 Bordes, France

Abstract

Blades vibrations must be measured in operations to validate blade design. Tip-timing is one of the classical measurement methods but its main drawback is the generation of sub-sampled and non-uniform sampled signals. Consequently tip-timing signals cannot be processed with conventional methods. Assuming that blade vibration signals yield to line spectra, we introduced a sparse signal model that uses speed variation of the engine. The usual solutions of inverse problems are given with the LASSO method. This paper presents a new approach based on a ℓ^0-regularization. It is solved with the OMP algorithm adapted to our model. Results from synthetic and real signals are presented to illustrate the efficiency of this method, including a real blade crack test case. The main advantages of the proposed method are to provide accurate estimations with a computational cost drastically reduced with respect to existing methods. Besides, the method does not need to set up regularization parameters while taking into account the speed variation of the engines. Finally, results show that this approach greatly reduces frequency aliasings caused by the low sampling frequency of the measured signals.

Keywords: Spectral analysis, Non uniform sampling, Blade vibration, Tip-timing, Sparse, Crack detection

1. Introduction

1.1. Blade vibration monitoring

Compressors and turbines blades vibrations measurements are a key element in the turbomachinery test certification campaign. Indeed, in operating conditions, blades are excited by alternating aerodynamic forces that may cause mechanical resonances. Compressors and turbines tests aim at identifying and quantifying such blades mechanical responses. Blades vibrations are traditionally measured by strain gauges, which are attached to the surface of the blades. Because of the centrifugal stresses, high aerodynamic pressure and functioning temperature, the gauges can quickly be damaged during a run. In addition, due to the high implementation cost and complexity, only a few blades are generally instrumented. Besides, sticking a gauge and its wire on a blade may slightly modify its mechanical response. All these gauges drawbacks made popular another measurement method, able of monitoring all the blades, less intrusive and easier to set up, called tip-timing [1]. The acquisition system is composed of a set of proximity sensors mounted on the stator and monitoring the blade tip passing times, see Figure 1. When a blade is passing in front of the laser beam, the optical probe detects the blade and records the corresponding time. This time can vary if the blade is vibrating and the delay can be interpreted as a blade tip displacement, via the instantaneous rotational frequency and the blade dimension knowledge. For example, on the Figure 1, the vibrating blade, indicated in blue, is ahead of its non-vibrating state, marked with the dotted line. This time advance is then interpreted as a positive amplitude, owing to the counter-clockwise rotation.

Email addresses: antoine.bouchain@centralesupelec.fr (Antoine Bouchain), jose.picheral@centralesupelec.fr (José Picheral), elisabeth.lahalle@centralesupelec.fr (Elisabeth Lahalle), gilles.chardon@centralesupelec.fr (Gilles Chardon), agathe.vercoutter@safrangroup.com (Agathe Vercoutter), arnaud.talon@safrangroup.com (Arnaud Talon)

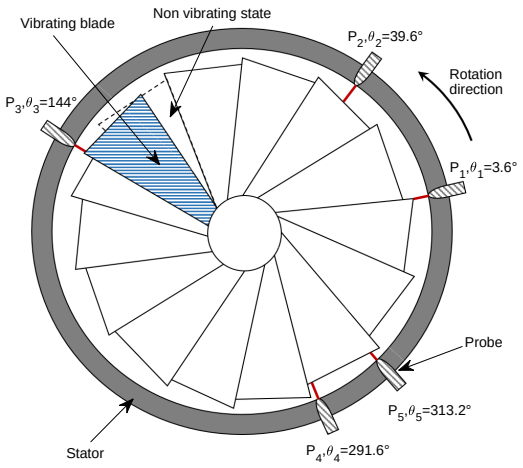


Figure 1: Blade vibration measurement with tip-timing technology.

It is important to note that the probes are non-equidistant due to geometrical constraints about the stator. These irregular probe positions generate irregular sampling times, as shown Figure 2. Moreover, this irregular sampling pattern is repeated at each revolution. Under the condition of a constant rotational frequency (F_r), the time sampling pattern is irregular and periodic. Thus, the frequency sampling pattern consists of peaks located at every multiple of the rotational frequency, in other words, frequency aliasing occurs with a periodicity of F_r. Most often, the frequencies of blades vibrations are largely higher than the rotational frequency. Consequently, blade tip-timing signals are sub-sampled and the spectra contain aliased components generated by the sampling patterns.

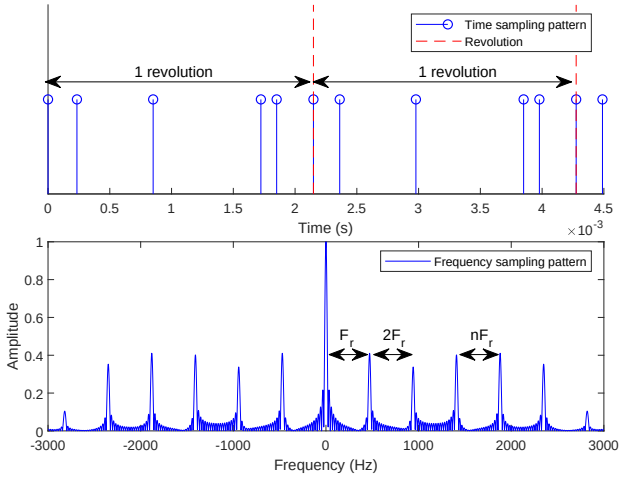


Figure 2: Example of tip timing non uniform sampling.

1.2. Spectral analysis with tip-timing signals

For the last 40 years, several solutions have been developed to face the difficulty of estimating blade vibrations from sub-sampled and irregular tip-timing signals [2, 3, 4, 5, 6]. However, the multi-components spectral analysis remains an open issue. Furthermore, most of the existing methods rely on strong assumptions about blade mechanical behaviour, such as an organised harmonic response, which are not necessarily confirmed in real functioning. Recently, new approaches that do not require such hypotheses have been proposed. Beauseroy *et al.* [7] proposed a spectrum

reconstruction from two subset of probes. As the location of the aliasing on the spectrum is probe position dependant, two subsets of probes produce different aliasing locations. Nevertheless, this process requires a small number of spectral components to estimate or a Signal to Noise Ratio (SNR) superior to 20 dB [8], which rarely occurs on real signals. In addition, this method does require that probes are regularly spaced, which is most often impracticable, as previously indicated. The Minimum Variance Spectral Estimator (MVSE) [9, 10, 11], is an iterative method which estimates the covariance matrix for Capon method [12] in the case of tip-timing signals. However, this method involves a high computation time and does not sufficiently cancel the aliasings on real data. Compressed sensing approaches have well performed in vibration analysis for non-uniform sampling signals. For instance, Lin *et al.* [13] propose a sparse reconstruction method that has been adapted to the tip-timing technology. Note that, inherent hypothesis of such method does not allow engine speed variations. In consequence, on real data, the rotation speed variations limit the length of the observation window and can lead to erroneous amplitudes estimations. A recent approach that takes into account the rotational frequency fluctuations has been developed [14], but, once again, this method requires uniform probes positions and the amplitude estimation is rather biased. Therefore, a ℓ^1-regularised method, developed in [15] by the authors, has been proposed for spectral analysis of tip-timing signals with engine speed rotation variations. The use of sparsity in the method is justified with the *a priori* knowledge that blades present a limited number of vibration modes on the engine range of use. As a result, the vibration signal spectrum consists of a very limited number of frequency lines. As far as line spectra of non-uniform sampled signals are concerned, they have already been studied with sparse methods (see [16], for instance). Nonetheless, in the context of tip-timing signals, the issue is slightly different since the frequency sampling pattern, see Figure 2, leads to numerous aliasings in the spectrum on the considered frequency range.

In this paper, we investigate the application of a spectral analysis method based on a simple structured sparsity model on the blade vibration spectrum. The Block-OMP algorithm [17] yields the frequencies and amplitudes of the blades vibrations modes. The proposed method distinguishes itself in four main interests:

1. to enforce the frequency sparsity of Power Spectral Density (PSD) estimations in order to reduce aliasing and obtain accurate estimations.
2. to provide blades vibrations spectra with low computational time.
3. to manage the rotation speed variations (which enables to increase the observation windows lengths and thus the accuracy).
4. to provide a more accurate representation of the spectrum than simple sparsity in the frequency domain thanks to the structured sparsity model (it also offers a slight improvement in computation complexity).

Results of the proposed method are compared with the ℓ^1-regularization performed by the Alternating Direction Method of Multipliers (ADMM) algorithm [18] as well as the classical MVSE algorithm [11] on synthetic and real signals.

This paper is organised as follows: the sparse model is introduced in section 2. Section 3 describes the proposed method. Section 4 presents the results and performances of the method applied for synthetic signals and real data acquired from a blade crack test case. The section 5 concludes the paper.

2. Sparse model of tip-timing signal

2.1. Tip-timing signal

Tip-timing signals are constructed from data obtained for each blade, from the discrete times given by the probes. In addition, an amplitude is obtained from each probe at each revolution n, with the following relation:

$$A = 2\pi R F_r(n) \Delta\tau, \tag{1}$$

where R is the distance from the blade base to the disk center, $F_r(n)$ is the rotational frequency at the n^{th} revolution, and $\Delta\tau$ is the delay between the blade tip-passing time without vibration, estimated from the rotational frequency, and the real blade passing time with vibration, measured by the probes.

In this paper, we assume that the rotational frequency F_r is not stationary, but varies slowly, allowing to consider it constant on a given revolution: $F_r(n) = 1/T_r(n)$, with $1 \leq n \leq N_t$. Besides, C probes are located around the stator

at positions θ_c, $1 \leq c \leq C$, that are non-uniform due to mechanical constraints. Sampling pattern is then irregular. For a given revolution n, the sampling times are:

$$t_k = \theta_c T_r(n)/2\pi + \sum_{i=1}^{n-1} T_r(i) \tag{2}$$

with $k = c + C(n-1)$. Assuming that the vibration signal of a unique blade is $x(t)$, N samples x_k of $x(t)$ at times t_k are recovered during the experiment:

$$x_k = x(t_k). \tag{3}$$

Over a window of length L, the vibration of a blade is assumed to be composed of N_f sinusoidal components in the frequency band of interest $[0, f_{max}]$ of constant frequencies and amplitudes (*i.e.* independent of time and rotational frequency). The asynchronous vibrations can be considered as sinusoids even with variations of rotational frequency. Moreover, the synchronous vibrations can be modeled as sinusoids as well, providing that a shorter signal length is used. Hence, the vibration signal $x(t)$ can be written as:

$$x(t) = \sum_{i=1}^{N_f} \alpha_i^0 \cos(2\pi f_i^0 t + \varphi_i^0) \tag{4}$$

or, equivalently,

$$x(t) = \sum_{i=1}^{N_f} \beta_i^0 \cos(2\pi f_i^0 t) - \gamma_i^0 \sin(2\pi f_i^0 t) \tag{5}$$

where β_i^0 and γ_i^0 are the real and imaginary parts of $\alpha_i^0 e^{i\varphi_i^0}$.

2.2. Non-uniform Fourier transform

In the case of a unique excited mode, the non-uniform Fourier transform (NUFT) of x,

$$X(f) = \sum_{k=1}^{K} x_k e^{-i2\pi t_k f}, \tag{6}$$

can be used to identify the frequency and the amplitudes of the mode, as it absolute value is maximal at the modal frequency. However, for multiple modes, the NUFT exhibits a large number of sidelobes of high amplitudes as is visible on Figure 4. In particular, the high sidelobes associated to a high amplitude modes are difficult to distinguish from the mainlobe of a mode of smaller amplitude. It is therefore impossible to estimate the blade modal parameters using the NUFT where multiple modes are excited.

2.3. Sparse model

In order to deal with the high amplitude sidelobes, a sparse model for the vector of samples $\boldsymbol{x}$ can be built. The interval $[0, f_{max}]$ is discretised onto a grid of M frequency points $f_m = \frac{m}{M} f_{max}$, with a frequency step small enough so that the model error is negligible compared to the measurement noise. The vector of samples $\boldsymbol{x}$ can be written as the following linear model:

$$\boldsymbol{x} = \boldsymbol{E_c}\boldsymbol{\theta_c} + \boldsymbol{E_s}\boldsymbol{\theta_s} + \boldsymbol{b} \tag{7}$$

$$= \boldsymbol{E}\boldsymbol{\theta} + \boldsymbol{b}, \tag{8}$$

where the matrices $\boldsymbol{E_c}$ and $\boldsymbol{E_s}$ are two dictionaries of cosines and sines, $\boldsymbol{E}$ their horizontal concatenation, and $\boldsymbol{\theta_c}$ and $\boldsymbol{\theta_s}$ are the coefficients of the expansion of x in these dictionaries, $\boldsymbol{\theta}$ their vertical concatenation. As only a few modes are excited, the number of nonzero coefficients of $\boldsymbol{\theta_c}$ and $\boldsymbol{\theta_s}$ is small compared to their dimension. Moreover, they share the same support.

These vectors and matrices are defined as follows:

$$
\begin{aligned}
\boldsymbol{x} &= [x(t_1)\ x(t_2)\ \dots\ x(t_N)]^T \text{ of size } [N \times 1] \text{ is the measured signal,} \\
\boldsymbol{\theta_c} &= [a_1^c\ a_2^c\ \dots\ a_M^c]^T \text{ of size } [M \times 1] \text{ are the amplitudes of the cosine terms to estimate,} \\
\boldsymbol{\theta_s} &= [a_1^s\ a_2^s\ \dots\ a_M^s]^T \text{ of size } [M \times 1] \text{ are the amplitudes of the sine terms to estimate,} \\
\boldsymbol{\theta} &= [\boldsymbol{\theta}_c^T \boldsymbol{\theta}_s^T]^T, \\
\boldsymbol{b} &= [b(t_1)\ b(t_2)\ \dots\ b(t_N)]^T \text{ of size } [N \times 1] \text{ is the unknown noise,} \\
\boldsymbol{E} &= [\boldsymbol{E_c}\ \boldsymbol{E_s}] \text{ is the dictionary with} \\
\boldsymbol{E_c} &= \begin{bmatrix} \cos(2\pi f_1 t_1) & \dots & \cos(2\pi f_M t_1) \\ \vdots & \dots & \vdots \\ \cos(2\pi f_1 t_N) & \dots & \cos(2\pi f_M t_N) \end{bmatrix} \text{ and} \\
\boldsymbol{E_s} &= \begin{bmatrix} -\sin(2\pi f_1 t_1) & \dots & -\sin(2\pi f_M t_1) \\ \vdots & \dots & \vdots \\ -\sin(2\pi f_1 t_N) & \dots & -\sin(2\pi f_M t_N) \end{bmatrix} \text{both of sizes } [N \times M].
\end{aligned}
$$

Notice that the definition of the model (8) with the dictionary $\boldsymbol{E}$ is based on the explicit sampling time. It requires that the sampling time are known, but the counter part is that it does not need any hypothesis on the rotational speed which can be varying.

3. Estimation of the model parameters

3.1. Criteria

The amplitudes $\boldsymbol{\theta}$ are estimated by solving (8), but as the number of unknowns is larger than the number of measurements, the linear system is under-determined. Sparsity constraints can be introduced to solve the system. Since $\{f_m\}_{m=1,\dots,M}$ are usually chosen to sample uniformly the frequency range of interest, $\boldsymbol{\theta}$ provides an estimation of the amplitudes a_m^c and a_m^S of each mode of frequency f_m and thus a spectral representation of the signal. As the number of excited modes is limited, most of the a_m^c and a_m^S are null so that $\boldsymbol{\theta}$ is sparse. This prior sparsity can be used as an additional constraint:

$$\hat{\boldsymbol{\theta}} = \underset{\boldsymbol{\theta}}{\operatorname{argmin}} \|\boldsymbol{x} - \boldsymbol{E\theta}\|_2^2 \text{ such that } \|\boldsymbol{\theta}\|_0 \leq K, \tag{9}$$

or as a penalization term:

$$\hat{\boldsymbol{\theta}} = \underset{\boldsymbol{\theta}}{\operatorname{argmin}} \|\boldsymbol{x} - \boldsymbol{E\theta}\|_2^2 + \lambda \|\boldsymbol{\theta}\|_0, \tag{10}$$

where $\|\boldsymbol{\theta}\|_0$ is the number of nonzero coefficients of $\boldsymbol{\theta}$, $K \in \mathbb{N}$ and $\lambda \in \mathbb{R}$. As these problems are non-convex and NP-hard, they cannot be solved exactly in a reasonable time frame.

A first approach is to replace the non-convex ℓ_0-"norm" by the convex ℓ_1-norm, yielding the LASSO estimator [19]:

$$\hat{\boldsymbol{\theta}} = \underset{\boldsymbol{\theta}}{\operatorname{argmin}} \|\boldsymbol{x} - \boldsymbol{E\theta}\|_2^2 + \lambda \|\boldsymbol{\theta}\|_1, \tag{11}$$

that can be solved using a wide variety of optimization algorithms such as linear programming, ISTA and FISTA [20], ADMM [18], *etc*. An application of this estimator to tip-timing monitoring was introduced in [15].

Another approach is to solve problem (9) approximately, *e.g.* using a greedy approach such as Orthogonal Matching Pursuit (OMP) [21], that identifies the nonzero coefficients of the decomposition iteratively. An iteration of OMP consists of two steps:

1. identification of the next non-zero coefficient, by selecting the atom of the dictionary the most correlated with the residual (here, as the atoms are sinusoids, this step amounts to find the maximal value of the NUFT of the residual).

2. projection of the vector to be decomposed onto the space orthogonal to the atoms identified so far, yielding the residual.

The iterations are stopped once a predetermined number of atoms are identified, or when the norm of the residual falls under a given threshold (*e.g.* the expected magnitude of the noise).

Here the vector of parameters $\boldsymbol{\theta}$ is not only known to be sparse, but also to exhibit a particular structure, as $\boldsymbol{\theta_c}$ and $\boldsymbol{\theta_s}$ share the same support. The block variant of OMP can take into account this additional structure [17]. Compared to the OMP algorithm, where the vector to be recovered is assumed to be the sum of a few vectors from a dictionary, here, a dictionary of subspaces is defined, and the vector to be recovered is assumed to be the sum of vectors taken from few of these subspaces. In our case, these subspaces are the spaces spanned by a cosine and a sine of identical frequencies.

Block-OMP algorithm

Ensure: $\mathscr{L}_0 = \emptyset$, $\boldsymbol{r_0} = \boldsymbol{x}$, $\boldsymbol{W_0} = []$
  while $k \leq K$ **do**
    • $\ell_k = \underset{\ell \in [1:M]}{\operatorname{argmax}} \|\Pi_{\boldsymbol{V_k}} \boldsymbol{r_{k-1}}\|_2$
    • $\mathscr{L}_k = \mathscr{L}_{k-1} \cup \ell_k$
    • $\boldsymbol{W_k} = [\boldsymbol{W_{k-1}}\ \boldsymbol{V_{\ell_k}}]$
    • $\boldsymbol{r_k} = \boldsymbol{x} - \Pi_{\boldsymbol{W_k}} \boldsymbol{x}$
    $k = k + 1$
  end while
  $\hat{\boldsymbol{\theta}} = \boldsymbol{W_K^\dagger x}$

Note: $\boldsymbol{V_k}$ is a basis of the k-th subspace of the dictionary, $\Pi_{\boldsymbol{V}}$ is the orthogonal projection on the set spanned by the vectors of $\boldsymbol{V}$.

The main difference with OMP occurs in the identification stage, where the selected subspace is the one that maximizes the norm of the orthogonal projection of the residual. However, in the case where the subspaces are all of dimension one, the identification step reduces to $\operatorname{argmax}_k\ |\boldsymbol{v_k^T r_{k-1}}|$, where $\boldsymbol{v_k}$ is the k-th unit vector of the dictionary, and Block-OMP reduces to OMP. The identification step involves an orthogonal projection onto a space of dimension two. The computation cost of this projection can be reduced by using the particular structure of the spaces as done in Appendix A.

3.2. OMP vs. Block-OMP

With OMP, it is not guaranteed that a mode at frequency f_0 will lead the identification of the cosine and sine at frequency f_0, as the sparsity is imposed independently on the cosine and sine coefficients ($\boldsymbol{\theta_c}$ and $\boldsymbol{\theta_s}$). This is caused by the non-orthogonality of the dictionary vectors and noise. By considering a dictionary of subspaces instead of vectors, Block-OMP ensures that pairs of sines and cosines are identified jointly. A drawback of Block-OMP is that the identification step involves orthogonal projections, more time-consuming than the scalar products involved in OMP. However, Appendix A shows that the particular structure of the dictionary allows a simple computation of these projections, making the identification step of Block-OMP slightly more time-consuming that an identification step of OMP, but less time-consuming than two identification steps necessary for OMP to locate a cosine-sine pair.

4. Numerical results

As a reminder, due to the irregular quasi-periodic sub-sampling, a tip-timing signal spectrum computed with classical spectral analysis such as the Non Uniform Fourier Transform (NUFT) provides numerous aliased components. Adapted methods are then truly required. Such methods must enable to distinguish real components among aliased ones and to estimate their amplitude accurately, with reasonable computation times. The following section presents, in two sub-parts, results on synthetic and real signals. The synthetic signal aims at estimating the performances of the proposed method in terms of MSE, aliasing cancellation and computation time. The results on real signal illustrate the method on a blade crack detection test case.

In the following two cases (synthetic and real signals), the proposed method is compared to:

- the NUFT, which is composed of many aliasings.
- the ADMM algorithm, which solves the LASSO problem (cf. (11)). It has the disadvantage of needing a calculation of the regularisation paramter λ. Further interesting results about the application of ADMM on tip-timing data are given in [15].
- MVSE method [9, 11] which is an acknowledged method for the tip-timing spectral analysis [22].

4.1. Synthetic signal: performances of the proposed estimator

Let us consider a synthetic signal whose characteristics are similar to real test cases. It is composed of three frequency components, $f_1^0 = 213$ Hz, $f_2^0 = 1626$ Hz and $f_3^0 = 1931$ Hz of respective amplitudes 10, 1 and 4. A white Gaussian noise is added whose variance is $\sigma^2 = \sigma^2_{f_2^0} 10^{-SNR/10}$, where the signal to noise ratio (SNR) is -10 dB and $\sigma^2_{f_2^0}$ is the power of f_2^0 component. The signal is generated with $C = 5$ probes at angular position 3.6°, 39.6°, 144°, 291.6° and 313.2° during $N_t = 200$ revolutions (the signal duration is about $0.42s$). Two cases are studied: one at constant rotational speed, the other at varying rotational speed. Rotational frequency variations are simulated with a $p = 12$ autoregressive (AR) process (fitted from real data) to which an acceleration trend is added ($\delta_{F_r} = 0.005$ Hz per revolution) from $F_r = 470$ Hz to 471 Hz. It is important to notice that f_1^0 aliasings will be located on f_2^0 since f_2^0 is $3F_r$ greater than f_1^0 ($f_2^0 - f_1^0 = 3 \times 471$ Hz). The acceleration trend may seem low but it is coherent with real data. Besides, the value is enough to modify the amplitude estimates as seen in [15].

Figure 3 and Figure 4 show the comparison of the spectral estimation provided by the proposed method (with Block-OMP), ADMM, MVSE, NUFT and Lin method (another sparse method [13]). The black crosses indicate the true amplitudes. The NUFT spectrum is showed to illustrate the necessity of using advanced methods to reduce the aliasings. The number of iterations is 50 for Block-OMP, 500 for ADMM and 5 for MVSE, which is enough to get a maximal absolute error inferior to 10^{-3} between two iterations. The regularization parameter for the LASSO problem is set to $\lambda = 1$. A grid of $M = 3000$ frequency points with a step of 1 Hz is used to represent the frequency band of interest between 0 and 2999 Hz.

Results on Figure 3 show that all methods, except the NUFT, estimate accurately the three components in the case of constant rotational speed. As expected, the NUFT spectrum is composed of numerous aliasings, hence, f_2^0 component is particularly badly estimated (due to the f_1^0 aliasings). The results for varying speed are plotted Figure 4 and the estimated amplitudes are summarised Table 1. The rotational speed variations may seem very small. However, even this variation of 1 Hz is enough for Lin method to fail to recover the exact amplitude owing to the rotational frequency variations which are not taken into consideration by this method. The other three methods deal correctly with varying speed and provide accurate estimates.

	$f_1^0 = 213$ Hz	$f_2^0 = 1626$ Hz	$f_3^0 = 1931$ Hz
True value	10	1	4
Block-OMP	10.13	1.03	4.03
ADMM	9.75	0.85	3.81
MVSE	10.04	0.98	4.03
NUFT	10.04	2.16	4.06
Lin	9.98	0	2.09

Table 1: Amplitude estimations of the synthetic signal.

The Mean Squared Error (MSE) of estimated amplitudes is evaluated for 100 noise independent realizations of previous signal. Only the MSE of f_2^0 component is plotted since it is the most difficult to estimate (due to the high amplitude of f_1^0 aliasings). Figure 5 gives the MSE versus SNR with a 200 revolutions signal length. As expected, the MSE decreases when SNR increases. But, more important, it can be observed that MSE of Block-OMP is lower than the MSE of MVSE (except for SNR = -15 dB) and ADMM. We also notice that the MSE of Block-OMP is slightly lower than the MSE of OMP. Figure 6 presents the signal length influence with $\sigma^2 = \sigma^2_{f_2^0}$. Beyond a certain signal

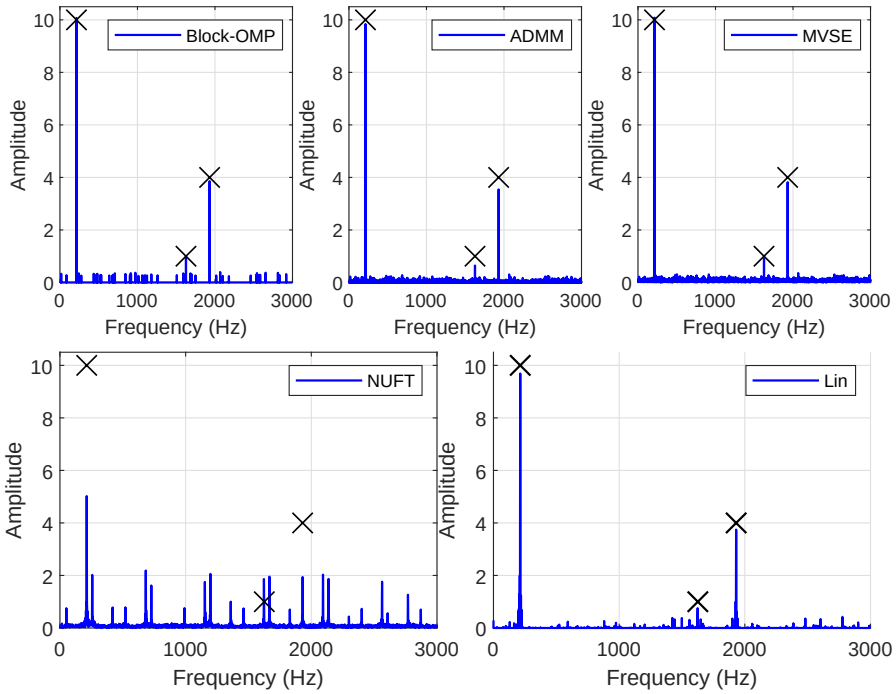


Figure 3: Synthetic signal spectra with OMP, ADMM, MVSE, NUFT and Lin (from left to right and top to bottom) at constant rotational speed.

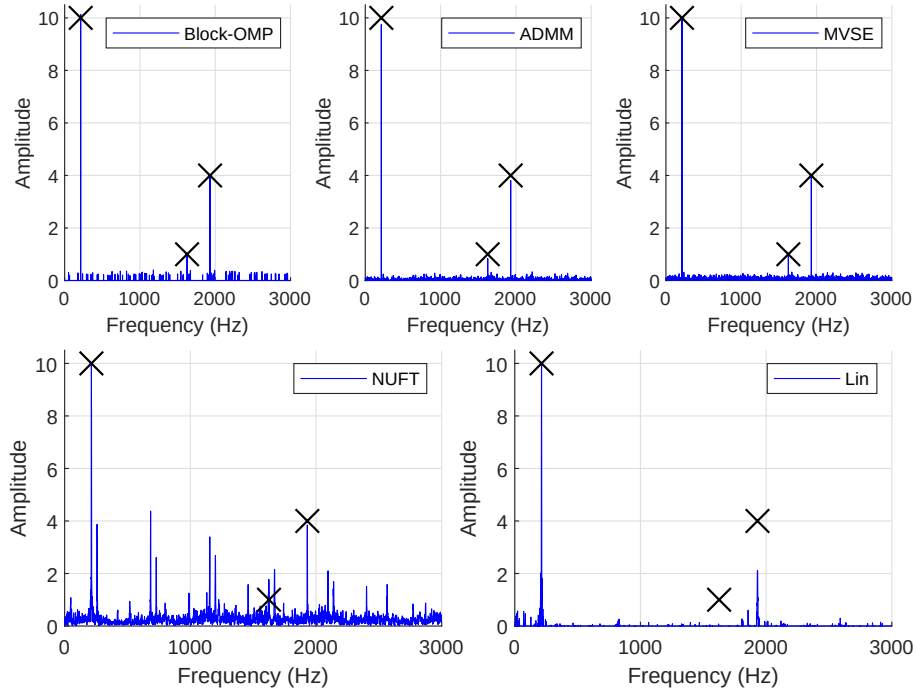


Figure 4: Synthetic signal spectra with OMP, ADMM, MVSE, NUFT and Lin (from left to right and top to bottom) at varying rotational speed.

length, about $0.42s$ in this example (that corresponds to 200 revolutions), Block-OMP provides the lowest MSE in comparison with the other methods. Once again, both OMP versions give very close results. We also mention that

due to excessive computation time, MVSE has not been calculated for the signal duration of $1.06s$ (500 revolutions).

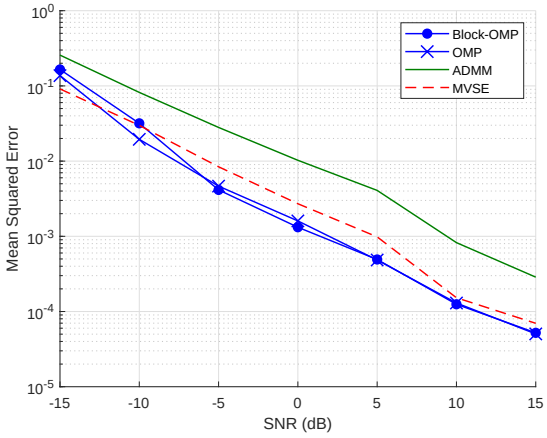


Figure 5: MSE of f_2^0 component of the synthetic signal for 200 revolutions.

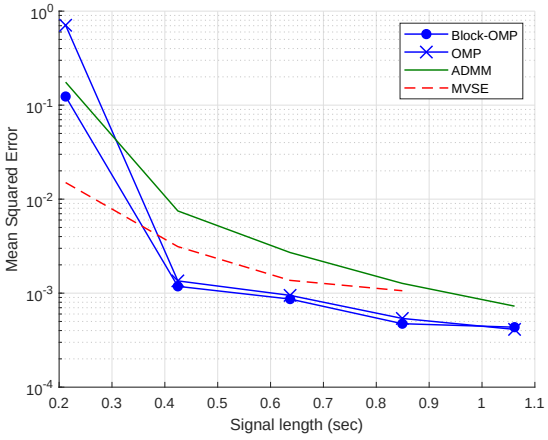


Figure 6: MSE of f_2^0 component of the synthetic signal for $\sigma^2 = \sigma^2_{f_2^0}$.

The performances in terms of aliasing cancellation are estimated by $S_{\tilde{y}}$, which is the ℓ^2-norm of the spectrum background (*i.e.* spectrum obtained by removing the three frequency components) and expressed as follows:

$$S_{\tilde{y}} = \sqrt{\sum_{m=1}^{M} |\hat{a}_m|^2 - \sum_{k=1}^{3} |\hat{a}_{m_k}|^2}, \tag{12}$$

where $\hat{a}_m$ are the estimates of $a_m = \sqrt{{a_m^c}^2 + {a_m^s}^2}$ and m_k are the indexes of the frequency components $\{f_k^0\}_{k=1,2,3}$ of the synthetic signals. Results of the methods for various signal length are given Figure 7 for $\sigma^2 = \sigma^2_{f_2^0}$. Beyond a signal length of $0.42s$ (200 revolutions), the MVSE spectrum is the less sparse while Block-OMP remains the sparsest. Furthermore, it is noticeable that the ADMM spectrum background does not decrease anymore but slightly increases, whereas the spectrum backgrounds of the two OMP versions still decrease. The OMP iterations number is directly linked to the sparsity and the estimation accuracy. However, even with a large number of iterations, about 16 times the number of frequency components in this example, Block-OMP gives the lowest background spectrum.

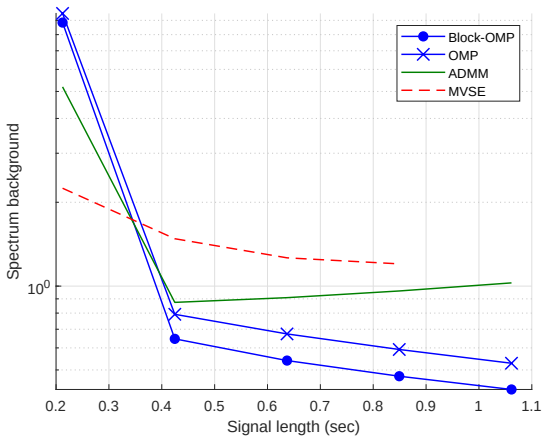


Figure 7: Signal length influence on the spectrum background ($S_{\tilde{y}}$).

The computation times of applicable methods, namely Block-OMP, ADMM and MVSE, are given Table 2 for different number of revolution. They have been computed under MATLAB® with an Intel® Core i7 processor unit cadenced at 2.5 GHz. It can be observed that the execution time increase, due to the signal length, is much less impacting for Block-OMP and ADMM than for MVSE. Note that Block-OMP for 500 revolutions is about 30 times faster than MVSE for 200 revolutions and provides more accurate estimation (see Figure 6). Block-OMP is unquestionably the fastest method whatever the number of revolutions.

Method \ Signal length	100 rev. (0.21s)	200 rev. (0.42s)	300 rev. (0.64s)	500 rev. (1.06s)
Block-OMP time (s.)	0.56	0.81	1.11	1.85
ADMM time (s.)	4.78	9.05	12.93	23.60
MVSE time (s.)	14.13	55.92	133.42	416.23

Table 2: Computation time (in seconds) for OMP, ADMM and MVSE.

The complexity of the algorithms, expressed as the number of additions and multiplications, namely for K iterations, are the following:

- Block-OMP: $O(KMN)$ and K usually equals to 50.
- ADMM: $O(KMN + MN^2)$ and K usually equals to 500.
- MVSE: $O(KMN^2)$ and K usually equals to 5.

With these numbers of calculations, we do understand why Block-OMP is the fastest: its signal length dependence is linear whereas it is quadratic for ADMM and MVSE.

4.2. Real signal

This part presents experimental results from real data. The real signal is extracted from data of an experimental compressor test rig with stabilised, but fluctuating, rotational frequency that is between 300 and 833 Hz. The tip-timing signal is measured with $C = 8$ optical probes located at 39.6°, 61.2°, 118.8°, 165.6°, 237.6°, 277.2°, 309.6° and 338°. The clock frequency is 80 MHz. During the test, a crack initiation on a blade seems to appear. Later, this event has been confirmed during the rig dismantlement: the crack spread on a single blade over several millimetres. The crack initiation results in an amplitude drop caused by the changes of the piece geometry. In addition, a modal frequency shift is observable during blade cracks [23, 24, 25]. The blades have a structure with cyclic symmetry and therefore all the modes are organised spatially around the axis of rotation. Nevertheless, the appearance of a crack breaks the symmetry of the structure which modifies the shape and the frequencies of the mode. A fall in frequency is observed as the crack spreads, and more particularly on the blade which cracks where we observe in addition an amplitude drop related to the dissipation that the crack engenders on the vibratory response of the blade. An asynchronous vibration of f_0 frequency is observable and corresponds to a rig mode frequency. This frequency f_0 is higher than the equivalent sampling frequency: $f_0 > f_e = CF_r$.

The Figures from 8 to 11 present the results of Block-OMP, ADMM, MVSE and NUFT methods respectively. Block-OMP and OMP are rather lookalike, hence, only the Block version is displayed. They are obtained with a signal of 40 000 revolutions divided into 400 windows of 200 revolutions duration and with 50% overlapping. On each window a spectrum is calculated with corresponding method. All the spectra are piled together to form a spectrogram for each method. The frequency grid step is 0.2 Hz for this signal. The normalised frequency 1 equals to CF_r where F_r is the average rotational speed. 50 iterations are used for Block-OMP, 100 for OMP, 500 for ADMM and 5 for MVSE. Amplitudes and frequencies have been normalised. The amplitude drop and the frequency shift occur right after the blade cracking at $t = 47s$. Block-OMP, OMP, ADMM and MVSE enable to easily identify the blade vibration frequency, since they provide a remarkable aliasing cancellation. Unlike the NUFT spectrogram, (Figure 11), where the vibration frequency is blended with the aliased frequency, making the spectral analysis impossible. Concerning the

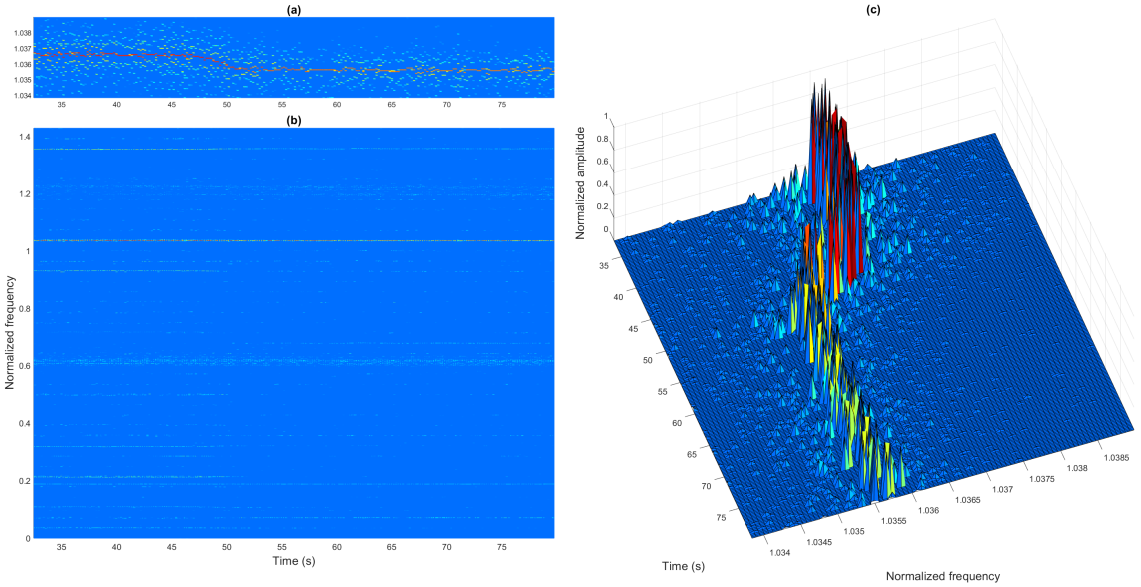


Figure 8: Block-OMP spectrogram: (a) is a zoom, on the frequency vibration, of the spectrogram (b) and (c) is the 3D view of the spectrogram, centred on the frequency vibration.

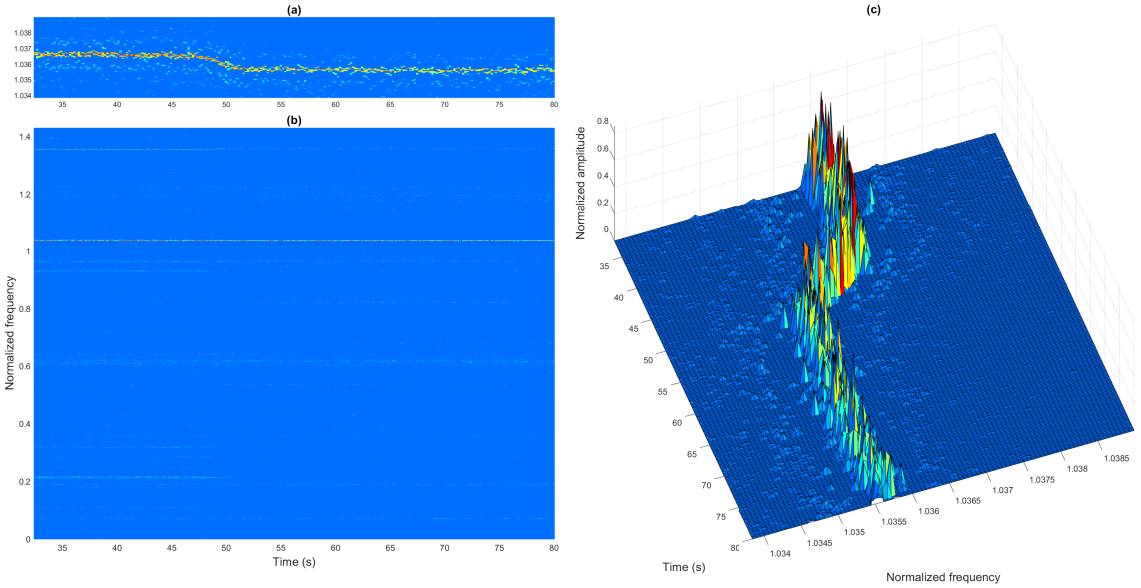


Figure 9: ADMM spectrogram: (a) is a zoom, on the frequency vibration, of the spectrogram (b) and (c) is the 3D view of the spectrogram, centred on the frequency vibration.

execution time, Block-OMP spectrogram required 17 min, OMP 19 min, ADMM 1h50 min, MVSE 27h and NUFT 2 min. The time saved with Block-OMP is particularly valuable in this case.

The blade vibration frequency and the corresponding amplitudes are extracted from the spectrograms. The results are displayed Figure 12 and Figure 13 which respectively plot the frequency and the amplitude trend. Frequencies and amplitudes are normalised and smoothed with a moving average of 3 seconds. As seen, regarding the frequency, the proposed method provides equivalent results compared to the other ones. Furthermore, the frequency shift, occurring

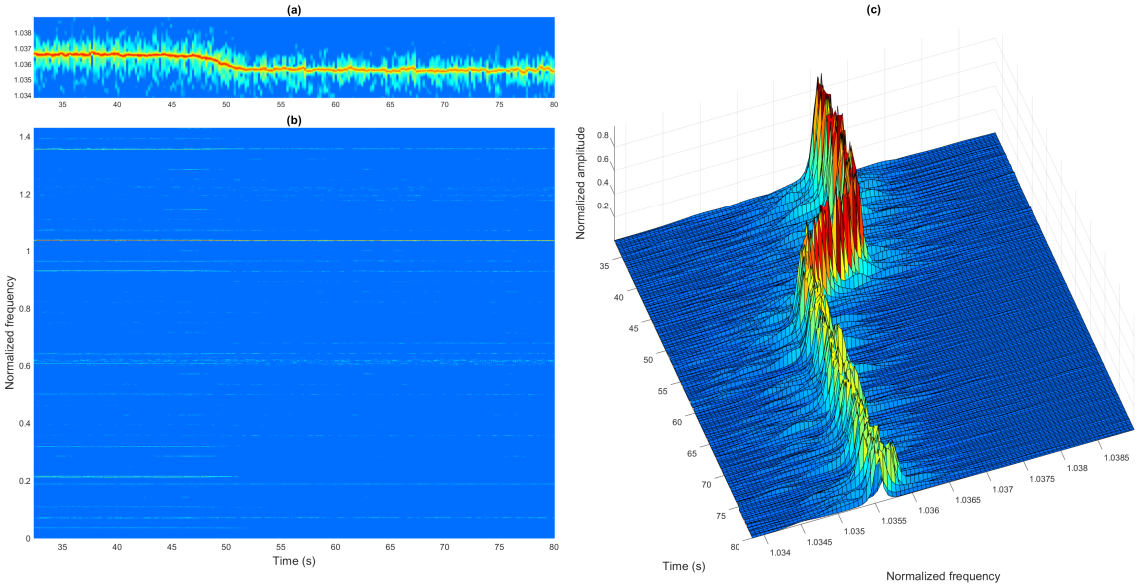


Figure 10: MVSE spectrogram: (a) is a zoom, on the frequency vibration, of the spectrogram (b) and (c) is the 3D view of the spectrogram, centred on the frequency vibration.

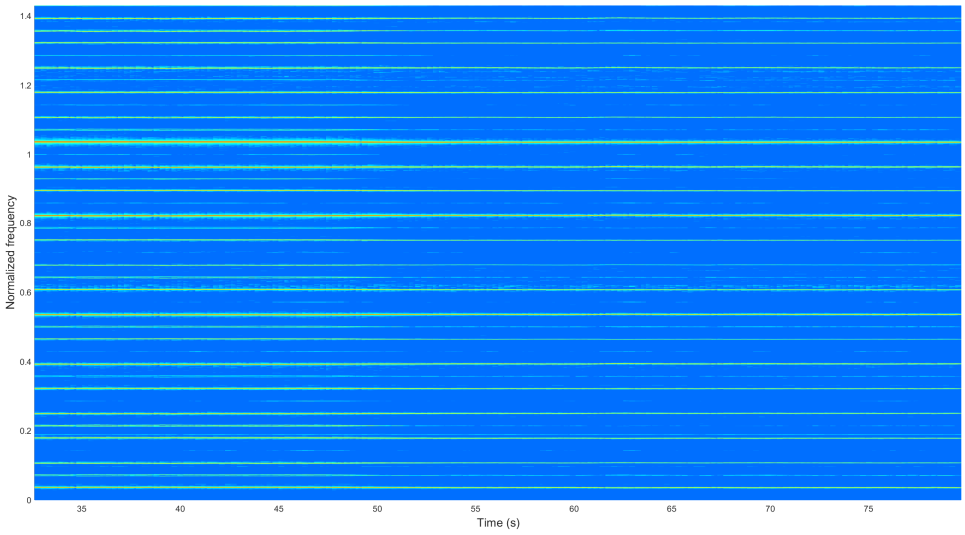


Figure 11: NUFT spectrogram.

during the blade crack initiation, is clearly shown with every method. Concerning the amplitudes, as mentioned earlier on the synthetic signal, the Block-OMP version and the classical OMP give close results, as well as MVSE. These amplitudes are also similar with those of the Circumferential Fourier Fit (CFF [26]) method from Hood Technology Corporation®. Contrary to the latter methods, ADMM amplitudes are much lower and much more saw-toothed. NUFT amplitudes are close to Block-OMP results (slightly over-estimated). However, we insist on the fact that NUFT spectrogram contains numerous aliasings, thus amplitudes could not be extracted without knowing the correct blade vibration frequency from other methods.

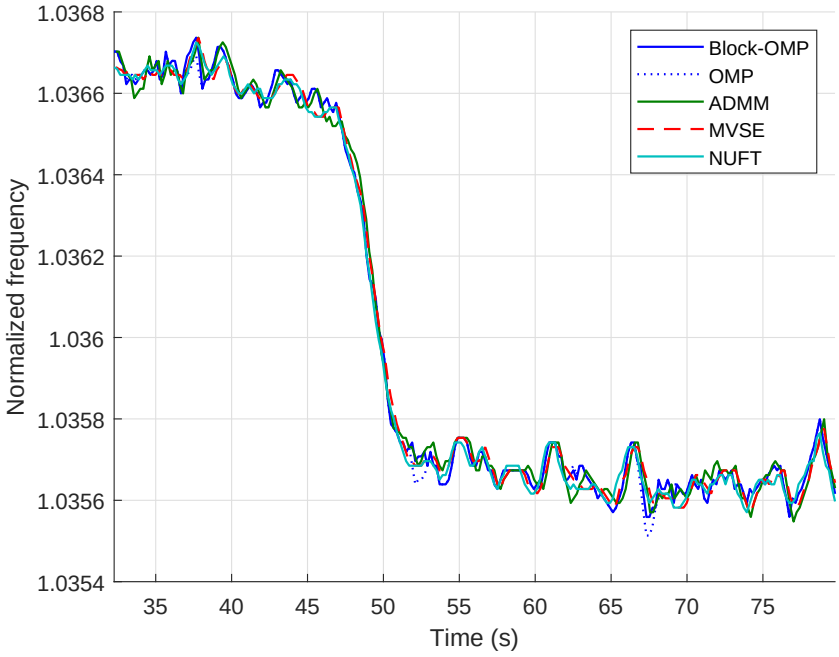


Figure 12: Frequency shift of the blade vibrating during the run.

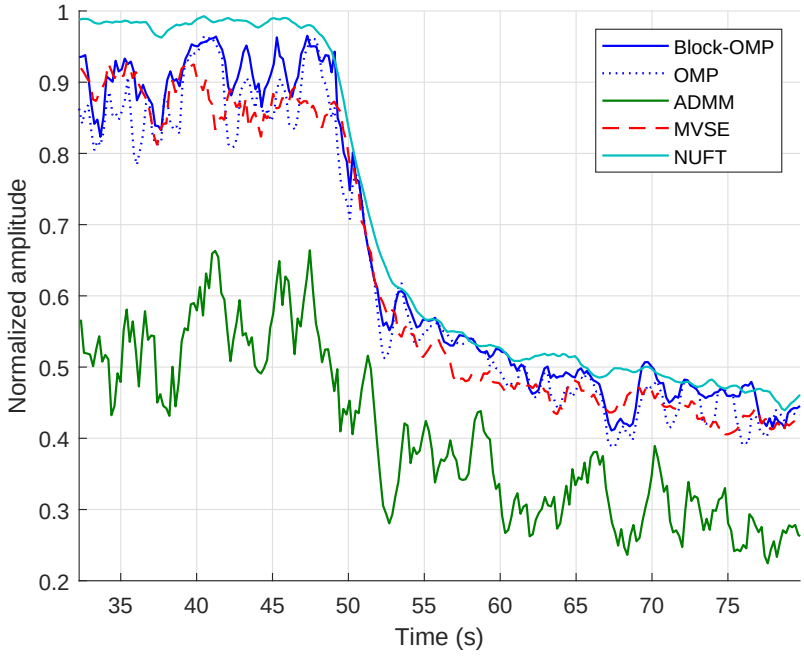


Figure 13: Amplitude drop of the blade vibrating during the run.

It is recalled that one of the main advantages of the tip-timing technology is to monitor all the blades at the same time. Thus, a Block-OMP spectrogram has been calculated for each blade of the compressor in the same test case.

Results are shown Figure 14 for four distinct blade behaviours, plus the cracking blade one. The left part of the figure is a zoom on the bandwidth of the blade vibration frequency. The right part plots the evolution of the extracted amplitudes at the same period. These plots give exhaustive information about all blade behaviours while one of them is cracking. They show that all the blades present a frequency shift after the cracking, but the evolution of the amplitudes is rather different. This real signal example truly highlights one of the best advantages of the tip-timing measurement method over the strain gauges. In such test cases, tip-timing measurements, while post-processed with adapted spectral methods, enable to analyse blade by blade vibration response at the same time and understand the overall mechanical behaviour.

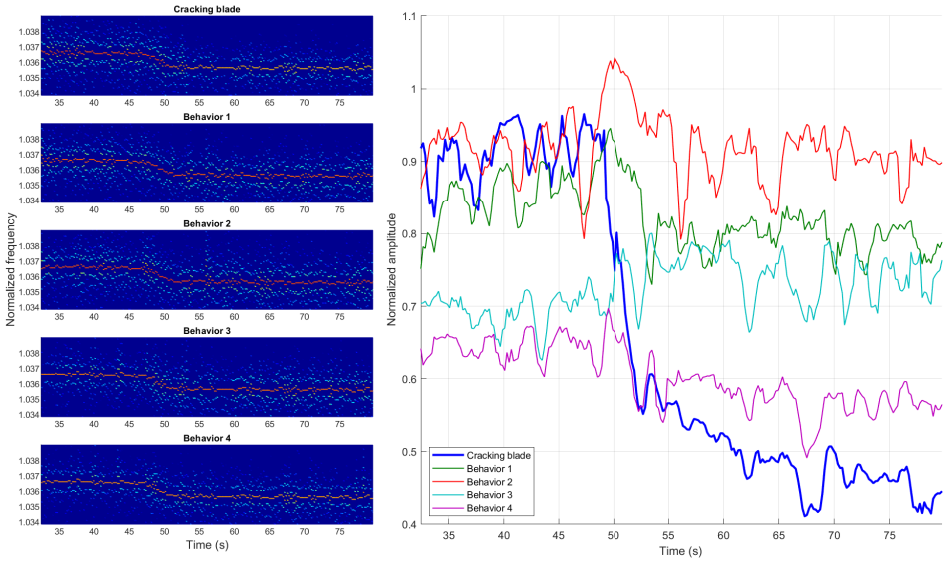


Figure 14: Distinct blade behaviours within the same compressor given by Block-OMP.

Furthermore, it is noteworthy that tip-timing can be used for crack detection monitoring. This topic has already been studied with the Non-Harmonic Fourier Analysis [24]. However, this method does require a regularly sampled signal as well as the knowledge of the crack frequency that needs to satisfy the Shannon's condition. Finally, due to the low execution time of the proposed method, an implementation in C® language, for instance, instead of MATLAB® could enable real time surveillance.

5. Conclusions and discussions

In this paper, we proposed a new PSD estimation method for analysing tip-timing signals. It is based on a time sparse model of the tip-timing signals that uses the real passing times, which take into account the rotational frequency variations. The proposed method minimises a criterion thanks to the Block-OMP algorithm, introducing ℓ^0-norm as sparsity prior. Numerical results show the interest of this method: aliasings are mainly cancelled and estimations are more accurate than existing methods. The fast execution time is valuable in order to extend the observation windows. It is an essential element, not only to reduce aliased components but also to improve the amplitude estimations, without being impacted by the engine rotation variations. The proposed method has also been validated on real data: similar results to existing methods are obtained with computational costs drastically reduced. This allows us consider real time applications, provided an efficient implementation. Despite the generation of sub-sampled and non-uniform sampled signals, tip-timing technology offers true advantages over the strain gauges. As seen on the blade crack test case, monitoring every blade and be able to analyse each one of them is very useful for understanding the compressor behaviour.

Appendix A. Identification step of Block-OMP

The identification step of Block-OMP needs the computation of the norm of the orthogonal projection of the residual $\boldsymbol{r}$ in the space spanned by a pair of vectors $\boldsymbol{u}_f$ and $\boldsymbol{v}_f$. Here $\boldsymbol{u}_f$ and $\boldsymbol{v}_f$ are a cosine and sine pair, and can be safely replaced by a pair of complex exponential of positive and negative frequencies. The projection $\boldsymbol{p}$ of $\boldsymbol{r}$ is given by:

$$\boldsymbol{p} = \boldsymbol{A}(\boldsymbol{A}^\star \boldsymbol{A})^{-1}\boldsymbol{A}^\star \boldsymbol{r}, \tag{A.1}$$

where $\boldsymbol{A} = [\boldsymbol{u}\ \boldsymbol{v}]$, and its norm is given by:

$$\|\boldsymbol{p}\|_2^2 = \boldsymbol{r}^\star \boldsymbol{A}(\boldsymbol{A}^\star \boldsymbol{A})^{-1}\boldsymbol{A}^\star \boldsymbol{r}. \tag{A.2}$$

The two dimensional vector $\boldsymbol{\rho} = \boldsymbol{A}^\star \boldsymbol{r}$ contains the values r_f and r_{-f} of the NUFT of $\boldsymbol{r}$ at the frequencies f and $-f$, that are conjugate of each other as $\boldsymbol{r}$ is a real vector. The vectors $\boldsymbol{u}_f$ and $\boldsymbol{v}_f$ are conjugate of each other and can assumed to be of norm 1, and the matrix $\boldsymbol{A}$ and its inverse can be written as:

$$\boldsymbol{A} = \begin{bmatrix} 1 & \gamma(f) \\ \gamma(f)^\star & 1 \end{bmatrix},\ \boldsymbol{A}^{-1} = \frac{1}{D(f)} \begin{bmatrix} 1 & -\gamma(f) \\ -\gamma(f)^\star & 1 \end{bmatrix} \tag{A.3}$$

where $\gamma(f) = \boldsymbol{u}_f^T \boldsymbol{v}_f$ and $D(f)$ is the determinant of $\boldsymbol{A}$. The norm of the projection is given by:

$$\|\boldsymbol{p}\|_2^2 = \frac{2}{D(f)} \left(|r_f|^2 - Re(\gamma^\star(f) r_f^2) \right). \tag{A.4}$$

The quantities $D(f)$ and $\gamma(f)$ can be computed *a priori*, and the norm of the projection $\boldsymbol{p}$ is obtained from the value of the NUFT of $\boldsymbol{r}$ at frequency f. Compared to standard OMP, two NUFTs are replaced by a NUFT followed by a low time-consuming post-processing.

Bibliography

[1] W. C. Nieberding, J. L. Pollack, Optical Detection of Blade Flutter, in: ASME 1977 International Gas Turbine Conference and Products Show, American Society of Mechanical Engineers, 1977, p. V001T01A064. doi:10.1115/77-GT-66.

[2] S. Heath, M. Imregun, An improved single parameter method for turbomachinery blade vibration measurements using optical laser probes, Journal of Mechanical Science (1996) 1047–1058.

[3] S. Heath, M. Imregun, A Survey of Blade Tip-Timing Measurement Techniques for Turbomachinery Vibration, J. Eng. Gas Turbines Power 120 (4) (1998) 784–791. doi:10.1115/1.2818468.

[4] M. Zielinski, G. Ziller, Noncontact vibration measurements on compressor rotor blades, Meas. Sci. Technol. 11 (7) (2000) 847. doi:10.1088/0957-0233/11/7/301.

[5] G. Dimitriadis, I. B. Carrington, J. R. Wright, J. E. Cooper, Blade Tip-timing Measurement of Synchronous Vibrations of Rotating Bladed Assemblies, Mechanical Systems and Signal Processing 16 (4) (2002) 599–622. doi:10.1006/mssp.2002.1489.

[6] H. Guo, F. Duan, J. Zhang, Blade resonance parameter identification based on tip-timing method without the once-per revolution sensor, Mechanical Systems and Signal Processing 66-67 (2016) 625–639. doi:10.1016/j.ymssp.2015.06.016.

[7] P. Beauseroy, R. Lengellé, Nonintrusive turbomachine blade vibration measurement system, Mechanical Systems and Signal Processing 21 (4) (2007) 1717–1738. doi:10.1016/j.ymssp.2006.07.015.

[8] A. Vercoutter, Contribution au développement d'une stratégie d'estimation spectrale des signaux tip-timing pour l'analyse des vibrations de pales de compresseurs, Ph.D. thesis, Université de Franche-Comté (2013).

[9] M. Greitans, Multiband signal processing by using nonuniform sampling and iterative updating of autocorrelation matrix, Proceedings of the 2001 International Conference on Sampling Theory and Application (2001) 5.

[10] A. Vercoutter, M. Berthillier, A. Talon, B. Burgardt, J. Lardies, Tip Timing Spectral Estimation Method For Aeroelastic Vibrations of Turbomachinery Blades, International Forum on Aeroelasticity and Structural Dynamics (IFASD) (2011) 9.

[11] A. Vercoutter, J. Lardies, M. Berthillier, A. Talon, B. Burgardt, Improvement of Compressor Blade Vibrations Spectral Analysis From Tip Timing Data: Aliasing Reduction, ASME, 2013. doi:10.1115/GT2013-96016.

[12] J. Capon, High-resolution frequency-wavenumber spectrum analysis, Proceedings of the IEEE 57 (8) (1969) 1408–1418. doi:10.1109/PROC.1969.7278.

[13] J. Lin, Z. Hu, Z.-S. Chen, Y.-M. Yang, H.-L. Xu, Sparse reconstruction of blade tip-timing signals for multi-mode blade vibration monitoring, Mechanical Systems and Signal Processing 81 (2016) 250–258. doi:10.1016/j.ymssp.2016.03.020.

[14] C. Zhan, Z. Chen, Z. Hu, Y. Yang, H. Hu, Nonlinear time transformation-based vibration signal reconstruction for blade tip-timing under rotation speed fluctuations, in: Prognostics and System Health Management Conference (PHM-Harbin), IEEE, 2017, pp. 1–5. doi:10.1109/PHM.2017.8079152.

[15] A. Bouchain, J. Picheral, E. Lahalle, A. Vercoutter, A. Talon, Sparse Method for Tip-Timing Signals Analysis with Non Stationary Engine Rotation Frequency, EUSIPCO, 2018 26th European Signal Processing Conference (EUSIPCO), 2018.
[16] S. Bourguignon, H. Carfantan, J. Idier, A Sparsity-Based Method for the Estimation of Spectral Lines From Irregularly Sampled Data, IEEE Journal of Selected Topics in Signal Processing 1 (4) (2007) 575–585. doi:10.1109/JSTSP.2007.910275.
[17] Y. C. Eldar, P. Kuppinger, H. Bolcskei, Block-Sparse Signals: Uncertainty Relations and Efficient Recovery, IEEE Transactions on Signal Processing 58 (6) (2010) 3042–3054. doi:10.1109/TSP.2010.2044837.
[18] S. Boyd, Distributed Optimization and Statistical Learning via the Alternating Direction Method of Multipliers, Foundations and Trends® in Machine Learning 3 (1) (2010) 1–122. doi:10.1561/2200000016.
[19] R. Tibshirani, Regression Shrinkage and Selection via the Lasso, Journal of the Royal Statistical Society. Series B (Methodological) 58.
[20] A. Beck, M. Teboulle, A Fast Iterative Shrinkage-Thresholding Algorithm for Linear Inverse Problems, SIAM Journal on Imaging Sciences 2 (1) (2009) 183–202. doi:10.1137/080716542.
[21] Y. Pati, R. Rezaiifar, P. Krishnaprasad, Orthogonal matching pursuit: Recursive function approximation with applications to wavelet decomposition, IEEE Comput. Soc. Press, 1993, pp. 40–44. doi:10.1109/ACSSC.1993.342465.
[22] V. Kharyton, G. Dimitriadis, C. Defise, A Discussion on the Advancement of Blade Tip Timing Data Processing, in: Volume 7B: Structures and Dynamics, ASME, Charlotte, North Carolina, USA, 2017, p. V07BT35A002. doi:10.1115/GT2017-63138.
[23] M. Witoś, On the Modal Analysis of a Cracking Compressor Blade, Research Works of Air Force Institute of Technology 23 (1) (2008) 21–36. doi:10.2478/v10041-008-0016-0.
[24] P. Neri, Bladed wheels damage detection through Non-Harmonic Fourier Analysis improved algorithm, Mechanical Systems and Signal Processing 88 (2017) 1–8. doi:10.1016/j.ymssp.2016.11.010.
[25] V. Mileshin, V. Fateev, A. Stepanov, Blade Fissure Determination by Means of Blade-Tip Timing System (2018) 9.
[26] P. Tappert, D. Losh, J. Shaju, M. Mercadal, Analyze Blade Vibration 7.5 User's Manual, Tech. rep., Hood Technology Corporation (Feb. 2014).